Meson-baryon scattering up to the next-to-next-to-leading order in covariant baryon chiral perturbation theory

Jun-Xu Lu,[1,2] Li-Sheng Geng,[1,*] Xiu-Lei Ren,[3] and Meng-Lin Du[4]

[1]*School of Physics and Nuclear Energy Engineering and International Research Center for Nuclei and Particles in the Cosmos and Beijing Key Laboratory of Advanced Nuclear Materials and Physics, Beihang University, Beijing 100191, China*

[2]*Groupe de Physique Théorique, IPN (UMR8608), Université Paris-Sud 11, Orsay 91406, France*

[3]*Ruhr-Universität Bochum, Fakultät für Physik und Astronomie, Institut für Theoretische Physik II, D-44780 Bochum, Germany*

[4]*Helmholtz-Institut für Strahlen- und Kernphysik and Bethe Center for Theoretical Physics, Universität Bonn, D-53115 Bonn, Germany*

(Received 12 February 2019; published 27 March 2019)

We study the scattering of a pseudoscalar meson off one ground state octet baryon up to the next-to-next-to-leading order in covariant baryon chiral perturbation theory (BChPT) with the extended-on-mass-shell scheme. We perform the first combined study of the pion-nucleon and kaon-nucleon scattering data in covariant BChPT and show that it can provide a reasonable description of the experimental data. In addition, we find that it is possible to fit the experimental baryon masses and the pion-nucleon and kaon-nucleon scattering data simultaneously at this order, thus providing a consistency check on covariant BChPT. We compare the scattering lengths of all the pertinent channels with available experimental data and those of the heavy baryon ChPT and infrared BChPT and discuss the convergence of SU(3) BChPT.

DOI: 10.1103/PhysRevD.99.054024

I. INTRODUCTION

Elastic meson-baryon scattering[1] is a fundamental process that not only can test our understanding of the strong interactions but also plays a relevant role in the studies of the properties of single and multibaryons [1]. For instance, one can derive from pion-nucleon scattering the nucleon sigma term, which is essential to understanding the quark flavor structure of the nucleon in the scalar channel and plays an important role in direct dark matter searches [2–4]. In addition, meson-baryon scattering also provides key inputs in the construction of the chiral baryon-baryon interactions and may affect the equation of state of dense matter at high densities and therefore help understand the so-called hyperon puzzle [5–8] in explaining the existence of two-solar-mass neutron stars [9,10]. Because of these and others, one has seen increasing theoretical interests, such as chiral perturbation theory (ChPT) [11–16] and lattice QCD [17,18], as well as experimental interest [19–23] in meson-baryon scattering in recent years.

ChPT, as a low-energy effective field theory of QCD, plays an important role in our understanding of the nonperturbative strong interaction physics [24–27]. In particular, it provides a model independent framework to describe the dynamics of the Nambu-Goldstone bosons interacting among themselves and with other hadrons containing light (u, d, and s) quarks. For comprehensive reviews, see, e.g., Refs. [28–33].

The constraints imposed by chiral symmetry and its breaking are the most stringent on the self-interactions of the Nambu-Goldstone bosons, and therefore, ChPT has the largest predictive power in the pure mesonic sector. In the one-baryon sector, its predictive power decreases because a larger number of unknown low energy constants (LECs) has to be introduced. As only a finite number of them appears in a particular process, this does not severely hamper its applicability.[2] A further complicating factor is the power counting breaking (PCB) issue. Namely, because of the large nonzero baryon masses m_0 in the chiral limit, lower order analytical terms appear in nominal higher order loop calculations, and therefore, a consistent power counting is lost [27]. In the past three decades, several solutions have been proposed. The most studied ones are the heavy baryon ChPT [29,35], the infrared regularization (IR) baryon ChPT [36], and the extended-on-mass-shell (EOMS) regularization baryon ChPT [37,38]. For a short summary and comparison of these different schemes, see, e.g., Ref. [39].

*lisheng.geng@buaa.edu.cn

[1]Throughout this work, mesons and baryons refer to the octet of Nambu-Goldstone bosons and the ground-state octet baryons, unless otherwise specified.

[2]A beautiful example is the study of Compton scattering [34], where no unknown LECs appear up to NNLO.

Although the EOMS BChPT has been successfully applied to study pion-nucleon scattering [40–46], it has not been applied to study kaon-nucleon, or more generally, meson-baryon scattering. Our present study aims to fill this gap. It is particularly timely given the extensive studies of baryon masses [47–51] and the recent attempt to construct baryon-baryon interactions using covariant BChPT [52–56] with the EOMS scheme. As mentioned above, meson-baryon scattering connects these studies and provides a nontrivial test of the consistency of BChPT.

This article is organized as follows. In Sec. II, we present the theoretical formalism and calculate meson-baryon scattering amplitudes up to the next-to-next-to-leading (NNLO) order. Here, we briefly explain the renormalization of the meson-baryon scattering amplitudes and the power-counting breaking issue and refer to previous studies for more details. Fitting results and discussions are presented in Sec. III, followed by a short summary and outlook in Sec. IV.

II. THEORETICAL FORMALISM

In this section, we explain in detail how to calculate the meson-baryon scattering amplitudes in covariant BChPT with the EOMS scheme. As pion-nucleon scattering has been studied in this framework previously [40–43], we will only highlight the new ingredients in extending the study from SU(2) to SU(3). For details similar to the SU(2) case, we refer the reader to Refs. [40–43].

A. Scattering amplitudes and partial wave phaseshifts

In the isospin limit, the standard decomposition of the meson-baryon scattering amplitude reads [27,57]

$$T_{\rm MB} = \bar{u}(p',s')\left[A + \frac{1}{2}(\not{q} + \not{q}')B\right]u(p,s), \tag{1}$$

where $p(p')$ and $q(q')$ are the momentum of the initial (final) baryons and mesons, respectively (see Fig. 1). Introducing the Mandelstam variables s, t, u, one can rewrite Eq. (1) in an alternative form,[3]

$$T_{\rm MB} = \bar{u}(p',s')\left[D + \frac{i}{m_i+m_f}\sigma^{\mu\nu}q'_\mu q_\nu B\right]u(p,s), \tag{2}$$

where $\sigma^{\mu\nu} = \frac{i}{2}[\gamma^\mu,\gamma^\nu]$ and $D = A + \frac{s-u}{2(m_i+m_f)}B$. However, as noted in Ref. [57], since the leading part of A and B may cancel each other, one better use B and D to perform the low energy expansion of the scattering amplitudes when extracting the PCB terms.

The above scattering amplitudes can be projected onto specific partial waves in the following form [1]:

$$f^{l\pm} = \frac{1}{2}(f_1^l + f_2^{l\pm}), \tag{3}$$

[3]This can be easily checked by noting that $\bar{u}[\gamma^\mu,\gamma^\nu]q_\mu q'_\nu u = (m_i+m_f)\bar{u}(\not{q}+\not{q}')u - (s-u)\bar{u}u$.

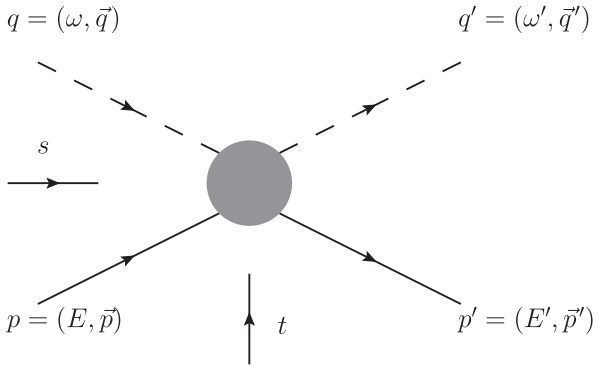

FIG. 1. Kinematics of meson-baryon scattering, where p, p', q, q' are the momenta of incoming and outgoing baryons and mesons, s and t are the Mandelstam variables. The solid lines denote baryons, and dashed lines represent mesons.

where f_1^l and f_2^l take the forms of

$$f_1^l = \frac{\sqrt{E+m_i}\sqrt{E'+m_f}}{8\pi\sqrt{s}}\left(A_l + \frac{\omega+\omega'}{2}B_l + \left(\frac{|\vec{q}|^2}{2(E+m_i)} + \frac{|\vec{q}'|^2}{2(E'+m_f)}\right)B_l\right), \tag{4}$$

$$f_2^l = \frac{\sqrt{E+m_i}\sqrt{E'+m_f}|\vec{q}||\vec{q}'|}{8\pi\sqrt{s}}\left(\frac{B_l}{2(E+m_i)} + \frac{B_l}{2(E'+m_f)} - \frac{A_l - \frac{\omega+\omega'}{2}B_l}{(E+m_i)(E'+m_f)}\right), \tag{5}$$

$$A_l(s) = \int_{-1}^{1} A(s,t)P_l(\cos\theta)d\cos\theta,$$
$$B_l(s) = \int_{-1}^{1} B(s,t)P_l(\cos\theta)d\cos\theta, \tag{6}$$

where E, E', ω, ω' are the energy of the incoming and outgoing particles in the center of mass (c.m.) frame, $\vec{q}$ and $\vec{q}'$ are the c.m. momentum of the incoming(outgoing) mesons, m_i and m_f are the masses of the incoming and outgoing baryons. The P_l above refers to the Legendre polynomials with an angular momentum l.

From the partial wave amplitudes, one can obtain the corresponding phase shifts [58],

$$\delta_{l\pm} = \arctan\{|\vec{p}|Ref_{l\pm}(s)\}. \tag{7}$$

In the present work, we will rely on the modern partial wave analysis of the George Washington University group [59,60] to fix the relevant LECs.[4]

[4]For pion-nucleon scattering, one may also use the latest analysis based on the Roy-Steiner equation [61]. However, as our primary interest is to compare different formulations of BChPT, we choose to use the same data to fix the relevant LECs as those used by the previous studies [16,42].

B. Power counting

In ChPT, the relative importance of a certain Feynman diagram contributing to a particular process is determined by its chiral order, ν, whose size is of the order of $(p/\Lambda_\chi)^\nu$, where p denotes a generic small quantity and Λ_χ the chiral symmetry breaking scale. In the one-baryon sector, where only one baryon is involved in both the initial and the final states, the chiral order for any given Feynman diagram with L loops, V_n nth order vertices, N_M internal meson lines, and N_B internal baryon lines, is

$$\nu = 4L + \sum_n nV_n - 2N_M - N_B. \tag{8}$$

In the present context, the small quantities or expansion parameters are

$$s - \tilde{m}^2 \sim \mathcal{O}(p), \qquad t \sim \mathcal{O}(p^2),$$
$$m_\pi, m_K, m_\eta \sim \mathcal{O}(p), \qquad m_{N,\Lambda,\Sigma,\Xi} - \tilde{m} \sim \mathcal{O}(p^2). \tag{9}$$

Note that although in principle $\tilde{m}$ here refers to m_0, the chiral limit baryon mass, in the study of πN and KN scattering, we set $\tilde{m} = m_N$.

C. Chiral Lagrangians

In order to calculate the meson-baryon scattering amplitudes up to the leading one-loop order, i.e., $\mathcal{O}(p^3)$, we need the following meson-meson and meson-baryon Lagrangians:

$$\mathcal{L}_{\rm eff} = \mathcal{L}^{(2)}_{MM} + \mathcal{L}^{(4)}_{MM} + \mathcal{L}^{(1)}_{MB} + \mathcal{L}^{(2)}_{MB} + \mathcal{L}^{(3)}_{MB}, \tag{10}$$

where the superscripts denote the chiral order. The lowest-order meson-meson Lagrangian is

$$\mathcal{L}^{(2)}_{MM} = \frac{F_0^2}{4}\langle D_\mu U (D^\mu U)^\dagger\rangle + \frac{F_0^2}{4}\langle \chi U^\dagger + U\chi^\dagger\rangle, \tag{11}$$

where $\chi = \mathrm{diag}(m_\pi^2, m_\pi^2, 2m_K^2 - m_\pi^2)$, $U(\phi) = u^2(\phi) = \exp(i\frac{\phi}{F_0})$, and F_0 is the chiral limit value of the pseudoscalar decay constant. The traceless 3×3 matrix contains the pseudoscalar fields,

$$\phi = \sqrt{2}\begin{pmatrix} \frac{1}{\sqrt{2}}\pi^0 + \frac{1}{\sqrt{6}}\eta & \pi^+ & K^+ \\ \pi^- & -\frac{1}{\sqrt{2}}\pi^0 + \frac{1}{\sqrt{6}}\eta & K^0 \\ K^- & \bar{K}^0 & -\frac{2}{\sqrt{6}}\eta \end{pmatrix}. \tag{12}$$

The next-to-leading order meson-meson Lagrangian relevant to our study has the following form:

$$\mathcal{L}^{(4)}_{MM} = L_4\langle D_\mu U (D^\mu U)^\dagger\rangle\langle \chi U^\dagger + U\chi^\dagger\rangle + L_5\langle D_\mu U (D^\mu U)^\dagger (\chi U^\dagger + U\chi^\dagger)\rangle. \tag{13}$$

The lowest order meson-baryon Lagrangian [62,63] is

$$\mathcal{L}^{(1)}_{\phi B} = \langle \bar{B}(i\gamma^\mu D_\mu - m_0)B\rangle + \frac{D/F}{2}\langle \bar{B}\gamma^\mu\gamma_5[u_\mu, B]_\pm\rangle, \tag{14}$$

where m_0 is the chiral limit baryon mass, the covariant derivative $D_\mu B = \partial_\mu B + [\Gamma_\mu, B]$, $\Gamma_\mu = \frac{1}{2}\{u^\dagger\partial_\mu u + u\partial_\mu u^\dagger\}$, and $u_\mu = i\{u^\dagger\partial_\mu u - u\partial_\mu u^\dagger\}$. The 3×3 traceless matrix contains the ground-state octet baryons fields,

$$B = \begin{pmatrix} \frac{1}{\sqrt{2}}\Sigma^0 + \frac{1}{\sqrt{6}}\Lambda & \Sigma^+ & p^+ \\ \Sigma^- & -\frac{1}{\sqrt{2}}\Sigma^0 + \frac{1}{\sqrt{6}}\Lambda & n^0 \\ \Xi^- & \Xi^0 & -\frac{2}{\sqrt{6}}\Lambda \end{pmatrix}. \tag{15}$$

The meson-baryon Lagrangian at order $\mathcal{O}(p^2)$ relevant to meson-baryon scattering has 14 terms of the following form [62–64]:

$$\begin{aligned}\mathcal{L}^{(2)}_{\phi B} =\ & b_D\langle \bar{B}\{\chi_+, B\}\rangle + b_F\langle \bar{B}[\chi_+, B]\rangle + b_0\langle \bar{B}B\rangle\langle\chi_+\rangle + b_1\langle \bar{B}[u^\mu,[u_\mu,B]]\rangle + b_2\langle \bar{B}\{u^\mu,\{u_\mu,B\}\}\rangle \\ & + b_3\langle \bar{B}\{u^\mu,[u_\mu,B]\}\rangle + b_4\langle \bar{B}B\rangle\langle u^\mu u_\mu\rangle + ib_5(\langle \bar{B}[u^\mu,[u^\nu,\gamma_\mu\vec{D}_\nu B]]\rangle - \langle \bar{B}\overleftarrow{D}_\nu[u^\nu,[u^\mu,\gamma_\mu B]]\rangle) \\ & + ib_6(\langle \bar{B}[u^\mu,\{u^\nu,\gamma_\mu\vec{D}_\nu B\}]\rangle - \langle \bar{B}\overleftarrow{D}_\nu\{u^\nu,[u^\mu,\gamma_\mu B]\}\rangle) + ib_7(\langle \bar{B}\{u^\mu,\{u^\nu,\gamma_\mu\vec{D}_\nu B\}\}\rangle - \langle \bar{B}\overleftarrow{D}_\nu\{u^\nu,\{u^\mu,\gamma_\mu B\}\}\rangle) \\ & + ib_8(\langle \bar{B}\gamma_\mu\vec{D}_\nu B\rangle - \langle \bar{B}\overleftarrow{D}_\nu\gamma_\mu B\rangle)\langle u^\mu u^\nu\rangle + ic_1\langle \bar{B}\{[u^\mu,u^\nu],\sigma_{\mu\nu}B\}\rangle + ic_2\langle \bar{B}[[u^\mu,u^\nu],\sigma_{\mu\nu}B]\rangle + ic_3\langle \bar{B}u^\mu\rangle\langle u^\nu\sigma_{\mu\nu}B\rangle \end{aligned} \tag{16}$$

with $\chi_\pm = u^\dagger\chi u^\dagger \pm u\chi^\dagger u$.

The meson-baryon Lagrangian contributing to $MB \to MB$ at order $\mathcal{O}(p^3)$ has 13 terms of the following form [62–64]:

$$\begin{aligned}\mathcal{L}^{(3)}_{MB} =\ & id_1(\langle \bar{B}\gamma_\mu\vec{D}_{\nu\rho}B[u^\mu,h^{\nu\rho}]\rangle + \langle \bar{B}\overleftarrow{D}_{\nu\rho}\gamma_\mu B[u^\mu,h^{\nu\rho}]\rangle) + id_2(\langle \bar{B}[u^\mu,h^{\nu\rho}]\gamma_\mu\vec{D}_{\nu\rho}B\rangle + \langle \bar{B}\overleftarrow{D}_{\nu\rho}[u^\mu,h^{\nu\rho}]\gamma_\mu B\rangle) + id_3(\langle \bar{B}u^\mu\rangle \\ & \times\langle h^{\nu\rho}\gamma_\mu\vec{D}_{\nu\rho}B\rangle - \langle \bar{B}\overleftarrow{D}_{\nu\rho}h^{\nu\rho}\rangle\langle u^\mu\gamma_\mu B\rangle) + id_4\langle \bar{B}[u_\mu,h^{\mu\nu}]\gamma_\nu B\rangle + id_5\langle \bar{B}\gamma_\nu B[u_\mu,h^{\mu\nu}]\rangle + id_6(\langle \bar{B}u_\mu\rangle\langle h^{\mu\nu}\gamma_\nu B\rangle - \langle \bar{B}h^{\mu\nu}\rangle\langle u_\mu\gamma_\nu B\rangle) \\ & + id_7(\langle \bar{B}\sigma_{\mu\nu}\vec{D}_\rho B\{u^\mu,h^{\nu\rho}\}\rangle - \langle \bar{B}\overleftarrow{D}_\rho\sigma_{\mu\nu}B\{u^\mu,h^{\nu\rho}\}\rangle) + id_8(\langle \bar{B}\{u^\mu,h^{\nu\rho}\}\sigma_{\mu\nu}\vec{D}_\rho B\rangle - \langle \bar{B}\overleftarrow{D}_\rho\{u^\mu,h^{\nu\rho}\}\sigma_{\mu\nu}B\rangle) \\ & + id_9(\langle \bar{B}u^\mu\sigma_{\mu\nu}\vec{D}_\rho Bh^{\nu\rho}\rangle - \langle \bar{B}\overleftarrow{D}_\rho u^\mu\sigma_{\mu\nu}Bh^{\nu\rho}\rangle) + id_{10}(\langle \bar{B}\sigma_{\mu\nu}\vec{D}_\rho B\rangle - \langle \bar{B}\overleftarrow{D}_\rho\sigma_{\mu\nu}B\rangle)\langle u^\mu h^{\nu\rho}\rangle + d_{48}\langle \bar{B}\gamma_\mu B[\chi_-,u^\mu]\rangle \\ & + d_{49}\langle \bar{B}[\chi_-,u^\mu]\gamma_\mu B\rangle + d_{50}(\langle \bar{B}u^\mu\rangle\langle \chi_-\gamma_\mu B\rangle - \langle \bar{B}\chi_-\rangle\langle u^\mu\gamma_\mu B\rangle), \end{aligned} \tag{17}$$

where $D_{\nu\rho} = D_\nu D_\rho + D_\rho D_\nu$ and $h_{\mu\nu} = D_\mu u_\nu + D_\nu u_\mu$.

For Born terms at $\mathcal{O}(p^3)$ and vertex corrections, we also need the following Lagrangian, which contributes to $B_1 \to M_1 B_2$ and has ten terms [62–64]:

$$\mathcal{L}^{(3)}_{\rm BMB} = d_{38}\langle \bar{B}u^\mu\gamma_5\gamma_\mu B\chi_+\rangle + d_{39}\langle \bar{B}\chi_+\gamma_5\gamma_\mu Bu^\mu\rangle + d_{40}\langle \bar{B}u^\mu\gamma_5\gamma_\mu B\rangle\langle\chi_+\rangle + d_{41}\langle \bar{B}\gamma_5\gamma_\mu Bu^\mu\rangle\langle\chi_+\rangle + d_{42}\langle \bar{B}\gamma_5\gamma_\mu B\rangle\langle u^\mu\chi_+\rangle + d_{43}\langle \bar{B}\gamma_5\gamma_\mu B\{u^\mu,\chi_+\}\rangle + d_{44}\langle \bar{B}\{u^\mu,\chi_+\}\gamma_5\gamma_\mu B\rangle + d_{45}\langle \bar{B}\{\chi_-,\gamma_5 B\}\rangle + d_{46}\langle \bar{B}[\chi_-,\gamma_5 B]\rangle + d_{47}\langle \bar{B}\gamma_5 B\rangle\langle\chi_-\rangle. \quad (18)$$

It should be noted that not all of the $\mathcal{O}(p^2)$ and $\mathcal{O}(p^3)$ terms contribute to a specific process. Particularly, for pion-nucleon and kaon-nucleon scattering, only 24 combinations out of the total 37 LECs contribute. They are tabulated in Table I.

For an explicit study of the matching between SU(3) and SU(2), we refer the reader to Refs. [14,65,66]. In doing so, one should note that the Lagrangians in Eqs. (16), (17), and (18) do not share the same Lorentz structures with those used in SU(2). To obtain the matching relations between the LECs in the SU(2) and SU(3) Lagrangians, the following relation between D_μ and the Dirac matrix γ_μ is needed, which reads

$$\bar{\Psi}A^\mu iD_\mu\Psi + \text{H.c.} \doteq 2m\bar{\Psi}\gamma_\mu A^\mu\Psi, \quad (19)$$

where A^μ is an external field, and the symbol $\doteq$ means equal up to terms of higher orders. Neglecting the possible higher order corrections, which is beyond our concern here, it is straightforward to reduce the SU(3) Lagrangians to those of their SU(2) counterparts. We notice that although the application of Eq. (19) only leads to differences of higher orders, which could be ignored from the point of view of effective field theories, it results in a reorganization of the scattering amplitudes when divided into A and B parts. As a consequence, the explicit expressions of the tree level diagrams will be different.

We would like to point out that compared to the nine free LECs in the πN channel in SU(2) [42], we find that only eight of them are actually independent. All of the LECs in Eq. (18), which correspond to the d_{16} and d_{18} terms of Ref. [42], do not contribute to the scattering amplitudes. In the $\mathcal{O}(p^3)$ Born diagrams, the contributions from the $d_{38,\ldots,44}$ terms are canceled by the corrections from vertex renormalization. The remaining part, containing d_{45}, d_{46}, d_{47}, can be absorbed into those of the $d_{48,\ldots,50}$ terms via

$$2m\bar{\Psi}\gamma_5\chi_-\Psi \doteq -\bar{\Psi}\gamma_5\gamma^\mu[iD_\mu,\chi_-]\Psi + \frac{g_A}{2}\bar{\Psi}[\not{u},\chi_-]\Psi, \quad (20)$$

where g_A refers to the axial-vector current coupling constant. The first term on the right-hand side will be canceled as the $d_{38,\ldots,44}$ terms do, while the second term is in the form of the $d_{48,\ldots,50}$ terms. Thus, in the final scattering amplitudes, only eight combinations of the LECs will survive, consistent with the HBChPT study [16].

In addition, we note that the b_5, b_6, b_7 terms in the Lagrangians [Eqs. (16) and (17)] are not symmetric under the exchange of the Lorentz indices μ, ν, while the b_8 term is. As a consequence, these four terms do not share the same expression. The same applies to the d_1, d_2, d_3 terms. Considering that the differences are two chiral orders higher, we supplement these terms with the terms with exchanged Lorentz indices to make these Lagrangians symmetric with respect to the exchange of Lorentz indices. For instance, the modified b_5 and d_3 terms finally utilized in our calculation read

$$\begin{aligned}\mathcal{L}_{b_5} &= i(\langle\bar{B}[u^\mu,[u^\nu,\gamma_\mu\vec{D}_\nu B]]\rangle - \langle\bar{B}\overleftarrow{D}_\nu[u^\nu,[u^\mu,\gamma_\mu B]]\rangle) \\ &\quad + i(\langle\bar{B}[u^\nu,[u^\mu,\gamma_\mu\vec{D}_\nu B]]\rangle - \langle\bar{B}\overleftarrow{D}_\nu[u^\mu,[u^\nu,\gamma_\mu B]]\rangle), \\ \mathcal{L}_{d_3} &= i(\langle\bar{B}u^\mu\rangle\langle h^{\nu\rho}\gamma_\mu\vec{D}_{\nu\rho}B\rangle - \langle\bar{B}\overleftarrow{D}_{\nu\rho}h^{\nu\rho}\rangle\langle u^\mu\gamma_\mu B\rangle) \\ &\quad - i(\langle\bar{B}h^{\nu\rho}\rangle\langle u^\mu\gamma_\mu\vec{D}_{\nu\rho}B\rangle - \langle\bar{B}\overleftarrow{D}_{\nu\rho}u^\mu\rangle\langle h^{\nu\rho}\gamma_\mu B\rangle). \end{aligned} \quad (21)$$

TABLE I. Independent (combinations of) LECs contributing to πN and KN scattering. For the sake of later references, we introduce $\alpha_{1,\ldots,8}$, $\beta_{1,\ldots,8}$, $\gamma_{1,\ldots,8}$ to denote different combinations of LECs.

πN	$KN_{I=0}$	$KN_{I=1}$
$\alpha_1 = b_1+b_2+b_3+2b_4$	$\beta_1 = b_3-b_4$	$\gamma_1 = b_1+b_2+b_4$
$\alpha_2 = b_5+b_6+b_7+b_8$	$\beta_2 = b_6-\frac{b_8}{2}$	$\gamma_2 = b_5+b_7+\frac{b_8}{2}$
$\alpha_3 = c_1+c_2$	$\beta_3 = c_1+\frac{c_3}{4}$	$\gamma_3 = c_2+\frac{c_3}{4}$
$\alpha_4 = b_0+\frac{b_D}{2}+\frac{b_F}{2}$	$\beta_4 = b_0-b_F$	$\gamma_4 = b_0+b_D$
$\alpha_5 = d_2$	$\beta_5 = d_1+d_2+d_3$	$\gamma_5 = d_1-d_2-d_3$
$\alpha_6 = d_4$	$\beta_6 = d_4+d_5+d_6$	$\gamma_6 = d_4-d_5+d_6$
$\alpha_7 = d_8+d_{10}$	$\beta_7 = d_7-d_8+d_{10}$	$\gamma_7 = d_7+d_8+d_{10}$
$\alpha_8 = d_{49}$	$\beta_8 = d_{48}+d_{49}+d_{50}$	$\gamma_8 = d_{48}+d_{49}-d_{50}$

D. Feynman diagrams up to $\mathcal{O}(p^3)$

1. Tree level terms

The tree level contributions up to $O(p^3)$ are shown in Fig. 2. In the present work, we focus on the πN and KN sectors, which can be organized into the following four isospin multiplets: $\pi N^{I=3/2,1/2}$ and $KN^{I=1,0}$. The calculation of the tree level counterterms and Born terms is rather straightforward, and the corresponding results are given in Appendixes A and B, respectively.

2. Mass insertion diagrams

Mass insertions are induced by the SU(3) breaking corrections to the chiral limit baryon mass m_0, which are of order $\mathcal{O}(p^2)$ and have the following explicit form:

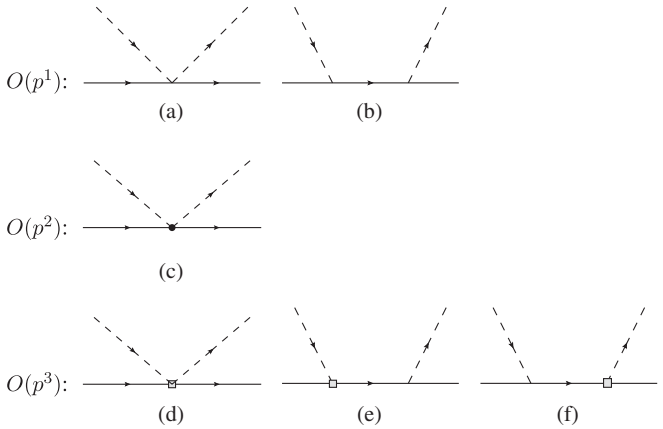

FIG. 2. Tree level diagrams contributing to meson-baryon scattering up to $O(p^3)$. The solid lines correspond to baryons, and the dashed lines represent mesons. The vertices with filled circles and hollow blocks stem from the $\mathcal{L}^{(2)}_{\rm MB}$ and $\mathcal{L}^{(3)}_{\rm MB}$ Lagrangians, respectively.

$$\begin{aligned}
\Delta_N &= -4{m_K}^2(b_0+b_D-b_F)-2{m_\pi}^2(b_0+2b_F),\\
\Delta_\Sigma &= -2{m_\pi}^2(b_0+2b_D)-4b_0{m_K}^2,\\
\Delta_\Lambda &= -\frac{2}{3}({m_K}^2(6b_0+8b_D)+{m_\pi}^2(3b_0-2b_D)),\\
\Delta_\Xi &= -4{m_K}^2(b_0+b_D+b_F)-2{m_\pi}^2(b_0-2b_F).
\end{aligned} \tag{22}$$

One easy way to include these corrections is to supplement the intermediate baryon mass of the Born terms with the $\mathcal{O}(p^2)$ corrections given in Eq. (22). The contribution from this part can be automatically included if one performs a substitution of $m_0 \to m_2 = m_0 + \Delta_B$ in the mass renormalization of baryons, as we do in this work.

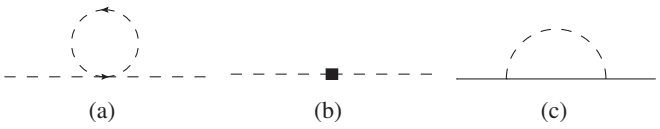

FIG. 4. Wave function renormalization contributions to meson (dashed) and baryon (solid) fields. Counterterms from $\mathcal{L}^{(4)}_{MM}$ are donated by the filled block.

3. Leading one-loop diagrams

The leading one-loop contributions to meson-baryon scattering include the Feynman diagrams shown in Fig. 3.

The crossed diagrams, if exist, can be obtained with the same replacement rule as in the case of the crossed Born diagrams,

$$\begin{aligned}
B_{\rm Loop} &= B(s) - B(s \leftrightarrow u, M_i \leftrightarrow M_f),\\
A_{\rm Loop} &= A(s) + A(s \leftrightarrow u, M_i \leftrightarrow M_f),
\end{aligned} \tag{23}$$

where $M_{i,f}$ refer to the masses of incoming and outgoing mesons. In the numerical evaluation of all these loop diagrams, we adopt physical values for all the quantities appearing in the amplitudes, including decay constants and masses. Employing their chiral limit values only lead to differences of higher chiral order.

The wave function renormalization of the external mesons and baryons are shown in Fig. 4, from which

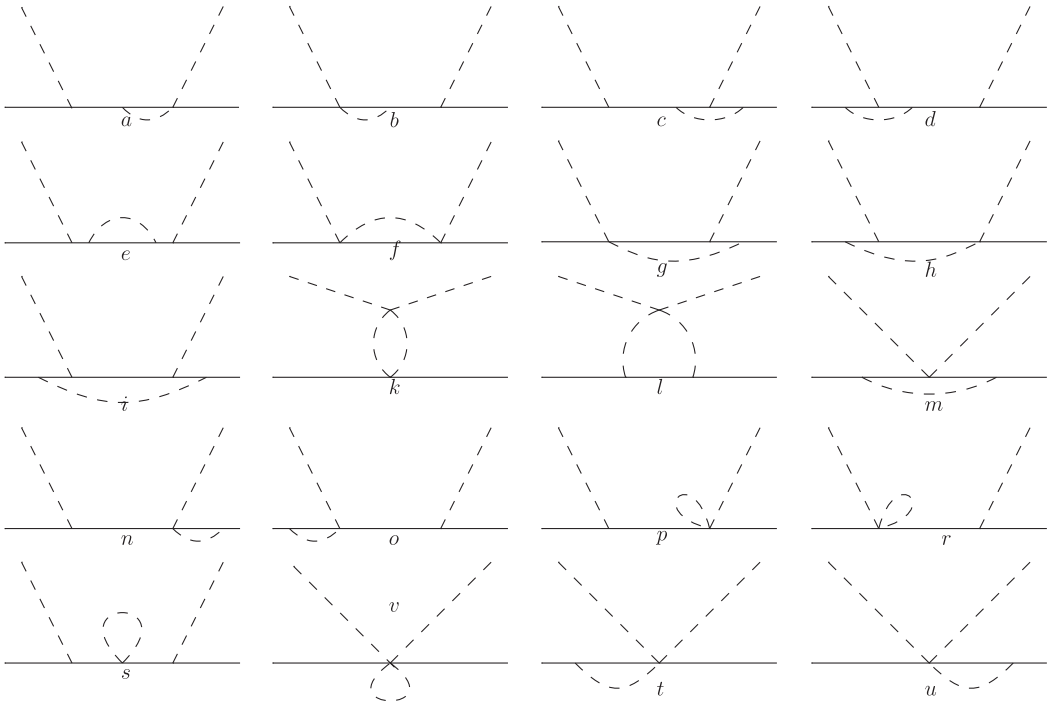

FIG. 3. Leading one-loop contributions to meson-baryon scattering up to $O(p^3)$. Note that the wave function renormalization and crossed graphs are not shown explicitly.

TABLE II. Eleven coupled channels of meson-baryon scattering of conserved strangeness (S) and isospin (I).

(1,1)	(1,0)	$(0,\frac{3}{2})$	$(0,\frac{1}{2})$	$(-1,2)$	$(-1,1)$	$(-1,0)$	$(-2,\frac{3}{2})$	$(-2,\frac{1}{2})$	$(-3,1)$	$(-3,0)$
KN	KN	$K\Sigma$	$K\Sigma$	$\pi\Sigma$	$\pi\Sigma$	$\pi\Sigma$	$\bar{K}\Sigma$	$\bar{K}\Sigma$	$\bar{K}\Xi$	$\bar{K}\Xi$
		πN	$K\Lambda$		$\eta\Sigma$	$\eta\Lambda$	$\pi\Xi$	$\bar{K}\Lambda$		
			ηN		$\pi\Lambda$	$\bar{K}N$		$\eta\Xi$		
			πN		$\bar{K}N$	$K\Xi$		$\pi\Xi$		
					$K\Xi$					

one can easily obtain the wave function renormalization constants for both meson and baryon external legs. For details we refer to Ref. [32].

In numerical calculations, we utilize the package OneLoop [67,68]. Due to the complexity of the explicit expressions of the one-loop contributions, they are not explicitly shown in this paper.[5]

The above obtained scattering amplitudes still need some further treatment before being employed to describe meson-baryon scattering. First, since in all the calculations above we used the physical values instead of the corresponding bare ones, the amplitudes must be properly renormalized. The procedure of renormalization is quite standard, see, e.g., Ref. [42]. We only need to point out that 1) the baryon mass normalization is implemented perturbatively and 2) the vertex renormalization is achieved via the two-body decay process, as in Ref. [43], and 3) the chiral corrections to decay constants are considered up to NLO [26]. To recover a proper power counting, we adopt the EOMS scheme.

We have checked our final results, particularly those of the loop functions, by reproducing the SU(2) phase shifts of Ref. [42] and the SU(3) scattering lengths of Ref. [12].

III. RESULTS AND DISCUSSION

The scattering of a pseudoscalar meson off an octet baryon can be grouped into 11 combinations of isospin and strangeness as tabulated in Table II. In the present work, we focus on the πN and KN channels, because only for these channels partial wave phase shifts are available.

With the amplitudes properly renormalized, we are now ready to determine the LECs by fitting to the partial wave phase shifts. For πN, we choose the phase shifts from the analysis of WI08 [59] in the $S_{11}, S_{31}, P_{11}, P_{31}, P_{13}, P_{33}$ partial waves, where in the convention $L_{2I,2J}$ L denotes the total orbit angular momentum, I the total isospin, and J the total angular momentum. Correspondingly, the phase-shift analysis of the SP92 solution [60] in the $S_{01}, P_{01}, P_{03}, S_{11}, P_{11}, P_{13}$ partial waves are used for KN, where the symbols mean $L_{I,2J}$.

For the πN channels, we choose the phase shifts with $\sqrt{s}$ between 1082 MeV, which is slightly above the threshold, and 1130 MeV, with an interval of 4 MeV. Thus, in total we will have 13 points for each of the six partial waves. For the KN channels, we follow the same strategy. Starting from 1435 MeV to 1475 MeV, the interval is set to be 2 MeV, with a total of 20 points for each partial wave.

Since WI08 does not provide the errors for the data, we follow Refs. [69,70] and take

$$\mathrm{err}(\delta) = \sqrt{e_s^2 + e_r^2\delta^2}, \tag{24}$$

with the systematic error $e_s = 0.1°$ and the relative error $e_r = 2\%$.

Throughout the numerical study, we use the physical decay constants for the corresponding vertices. The renormalization scale μ in the loop integrals is chosen to be the average mass of the baryon octet, and the $\tilde{m}$, appearing in the power counting breaking terms via $s - \tilde{m}^2$, is taken to equal to the mass of the nucleon, considering that we focus now on the πN and KN channels. The physical values employed in the present work are collected in Table III.

TABLE III. Masses and decay constants (in units of GeV) and axial-coupling constants relevant in the present work. Note the mass of the K meson is taken to be 0.493 GeV to be consistent with the SP92 data, which were originally from K^+n scattering.

m_π	m_K	m_η	m_N	m_Λ	m_Σ	m_Ξ
0.139	0.493	0.54765	0.939	1.1157	1.1934	1.3183

F_π	F_K	F_η	D	F	μ	$\tilde{m}$
0.0924	0.11003	0.11088	0.8	0.467	1.16	$m_N = 0.939$

A. Fitting strategy one: Direct fit to the phase shifts

We find that to describe the pion-nucleon scattering data, one needs to go to at least $\mathcal{O}(p^3)$. On the other hand, a reasonable reproduction of the kaon-nucleon data can already be achieved at $\mathcal{O}(p^2)$. We follow the same strategy in the first attempt to provide a simultaneous fit of both the πN and KN data.[6]

A least-of-squares fit yielded a $\chi^2/\mathrm{d.o.f.} = 0.154$ for the 78 data points in the pion-nucleon channel (see Table IV).

[5]They can be obtained from the authors upon request.

[6]As a matter of fact, different LECs contribute to πN and KN scattering independent of each other.

TABLE IV. LECs in the πN channel.

α_1 [GeV^{-1}]	α_2 [GeV^{-2}]	α_3 [GeV^{-1}]	α_4 [GeV^{-1}]	α_5 [GeV^{-4}]	α_6 [GeV^{-2}]	α_7 [GeV^{-3}]	α_8 [GeV^{-2}]	χ^2/d.o.f.
−7.63(6)	1.42(2)	1.34(1)	−1.36(6)	0.61(2)	3.25(5)	1.45(3)	−0.32(13)	0.154

The corresponding fit results associated with errors propagated from the uncertainties of LECs are compared with the empirical data in Fig. 5. For the sake of comparison, we show as well the $\mathcal{O}(p^3)$ results of the SU(3) HB [15,16] and the SU(2) EOMS BChPT [42].

Clearly, the EOMS results can describe the phase shifts quite well. Although the data are only fitted up to $\sqrt{s} = 1.13$ GeV, the phase shifts are described very well even up to $\sqrt{s} = 1.16$ GeV for some partial waves, corresponding to a momentum in the laboratory frame of $|\vec{p}_{\rm lab}| = 200$ MeV. In addition, our calculation in SU(3) shows a compatible description compared to that in SU(2), which implies that the inclusion of strangeness has small effects on the fitting results.

We note that even with the relative large uncertainties, we cannot achieve a satisfying description of the P_{11}, P_{13}, and P_{33} partial waves at higher energy regions. Particularly, in the P_{11} channel, the solution of WI08 tends to increase with energy in the higher energy region while the EOMS results, both in the SU(3) and SU(2) cases, decrease. This disagreement has already been noted in Ref. [42], where the authors point out that including the contribution of the $\Delta(1232)$ may improve the description. Inspired by this, we have checked that in SU(3) the inclusion of the lowest order contribution from the decuplet can have the same positive effect. One can achieve a pretty good description even up to $\sqrt{s} = 1.2$ GeV, quite close to the region of the Δ resonance. For a description bridging over this Δ resonance region, one needs to include the Δ explicitly, unitarize the amplitudes, and modify the powering counting rule. For a discussion of these, we refer the reader to Ref. [43].

For the KN scattering, as noted in the HB study [15,16], a quite good description of the phase shifts can already be achieved at NLO. In the present work, we will present two studies of the KN scattering. One is performed up to $\mathcal{O}(p^2)$, and the other is performed up to $\mathcal{O}(p^3)$, but only the loop contributions are included because the phase shifts data are not enough to fix the relevant $\mathcal{O}(p^3)$ LECs. Other inputs in addition to the KN phase shifts are needed. The second study will be denoted by $\mathcal{O}(p^3)^*$.

In Fig. 6, we show our fitted results together with the experimental data, with the corresponding LECs given in Tables V and VI. We find that in the KN channels, the error bands are very narrow for both the $\mathcal{O}(p^2)$ and $\mathcal{O}(p^3)^*$ results. In most partial waves, they are only a few percent of the corresponding phase shifts. For the sake of comparison, we show as well the HB results of Refs. [15,16]. It is clear that the EOMS descriptions are slightly better than the HB results when extended to higher energies.

From the above discussions, it is clear that the EOMS provides a satisfactory description of both the pion-nucleon

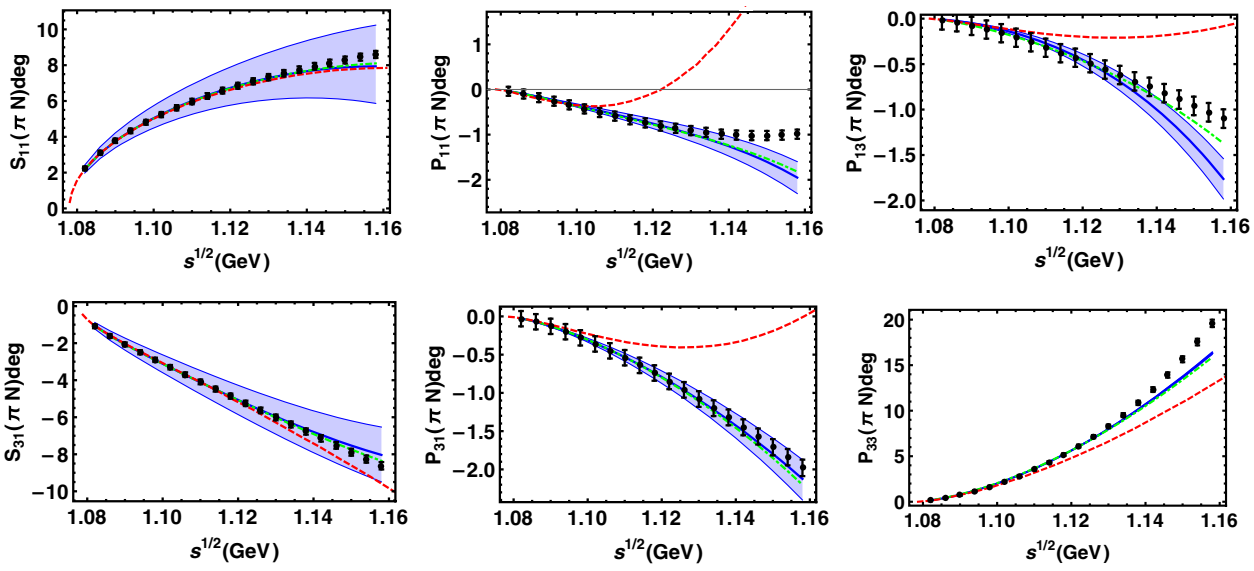

FIG. 5. Pion-nucleon phase shifts. The blue lines denote our results and the black dots with error bars represent the WI08 solution with empirical errors given in Eq. (24). The blue bands correspond to the uncertainties propagated from the uncertainties of the LECs. In some partial waves, the error bands are of the size of the thickness of the lines. For the sake of comparison, we show as well the EOMS SU(2) results [42] (green dot-dashed lines) and the HB SU(3) results [16] (red dashed lines).

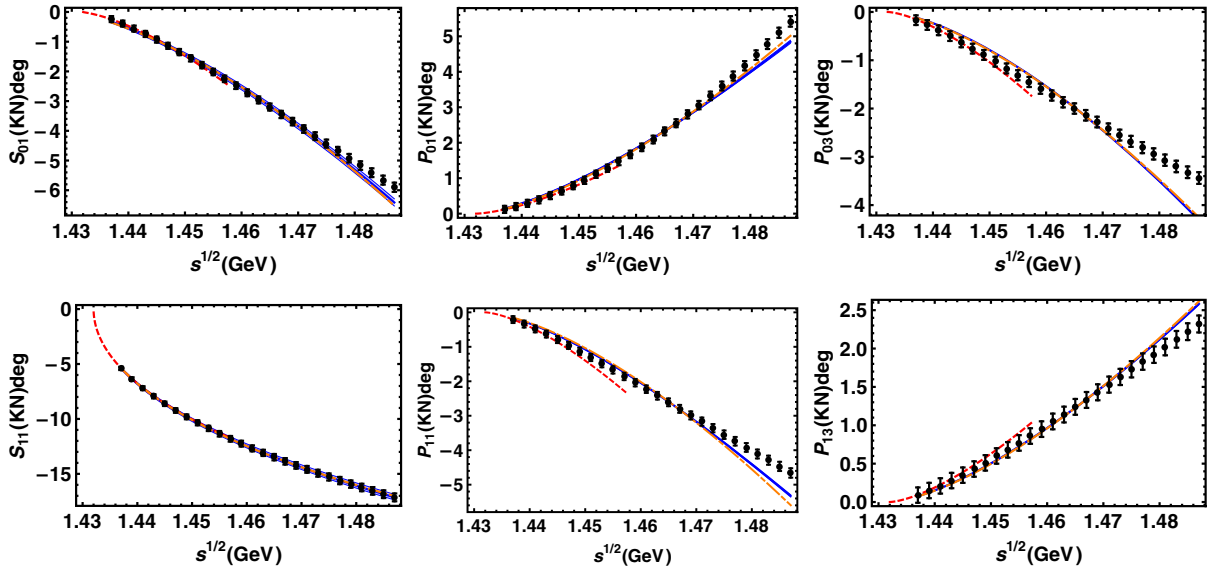

FIG. 6. $I = 0$ (upper panel) and $I = 1$ (lower panel) KN phase shifts. The orange long-short dashed lines and blue solid lines represent our $\mathcal{O}(p^2)$ and $\mathcal{O}(p^3)^*$ results while the red dashed lines denote those of the HB ChPT [16]. The blue bands correspond to the uncertainties of the $\mathcal{O}(p^3)^*$ results propagated from the uncertainties of the LECs. The error bands of the $\mathcal{O}(p^2)$ results are not shown here to make the figures easier to read. In some partial waves, the error bands are of the size of the thickness of the lines.

and kaon-nucleon scattering data up to $\mathcal{O}(p^3)$, while the SU(3) HB ChPT fails.

B. Fitting strategy two: Combined study of the baryon masses and meson-baryon scattering

One merit of ChPT is that it connects different observables with the same set of LECs. Thus, it is interesting to explore how one observable imposes restrictions on others. In this covariant baryon ChPT framework, baryon masses and scattering process are such a pair of observables which are described by the same Lagrangians. Most of the LECs appear in both the meson-baryon scattering and the baryon masses, such as, b_0, b_D, b_F, and $b_{1,\ldots,8}$. A naive idea for a combined study of these two observables can be performed in two ways. First, calculating baryon masses at $\mathcal{O}(p^3)$ and using the experimental data as well as the pion-nucleon sigma term to constrain b_0, b_D, b_F, and then with these LECs fixed, study pion-nucleon and kaon-nucleon scattering. Or conversely, one can study the baryon masses with some LECs determined via meson-baryon scattering and, furthermore, make predictions on sigma terms.[7]

However, we note that the LECs actually contribute at different chiral orders to these two observables. In meson baryon scattering, all of these LECs appear at $\mathcal{O}(p^2)$, the order of the chiral Lagrangians. On the other hand, b_0, b_D, b_F contribute to the baryon masses both at $\mathcal{O}(p^2)$ and $\mathcal{O}(p^4)$ via tree level as well as mass insertions, while $b_{1,\ldots,8}$ only contribute to the baryon masses via tadpole diagrams at $\mathcal{O}(p^4)$. This complicates things a lot. In principle, from the point of view of effective field theories, to achieve a fully self-consistent and combined study of baryon masses and meson-baryon scattering, one needs to renormalize the LECs in the same framework. In other words, the calculation for baryon masses and meson-baryon scattering ought to be performed up to the same order. Otherwise, the LECs in these two sectors are mismatched. Thus, if one tries to determine $b_{1,\ldots,8}$ through baryon masses, a calculation up to $\mathcal{O}(p^4)$ will be needed, which should be matched with scattering amplitudes also at $\mathcal{O}(p^4)$. As a consequence, the number of LECs will be too large compared with the number of data available both for baryon masses and meson-baryon scattering from experiments and lattice QCD simulations. On the other hand, if one is not so ambitious and only calculates the scattering amplitudes and baryon masses up to $\mathcal{O}(p^3)$, new problems show up. In this case, only three parameters(b_0, b_D, b_F) in

TABLE V. LECs contributing to the $I=0$ KN scattering.

	β_1 [GeV^{-1}]	β_2 [GeV^{-2}]	β_3 [GeV^{-1}]	β_4 [GeV^{-1}]	χ^2/d.o.f.
$\mathcal{O}(p^2)$	−0.495(1)	0.113(0)	0.447(2)	0.136(1)	0.829
$\mathcal{O}(p^3)^*$	−0.767(1)	0.126(0)	0.604(3)	0.093(1)	0.971

TABLE VI. LECs contributing to $I=1$ KN scattering.

	γ_1 [GeV^{-1}]	γ_2 [GeV^{-2}]	γ_3 [GeV^{-1}]	γ_4 [GeV^{-1}]	χ^2/d.o.f.
$\mathcal{O}(p^2)$	−0.122(0)	0.0084(0)	0.264(1)	−0.270(1)	0.765
$\mathcal{O}(p^3)^*$	−0.419(2)	0.429(0)	0.616(1)	−0.090(3)	0.471

[7]One can of course calculate the sigma terms directly from scattering amplitudes via the corresponding subthreshold parameters using the Cheng-Dashen theorem [71].

TABLE VII. LECs determined by fitting to the experimental baryon masses up to NLO in the EOMS BChPT and the corresponding fitted results, in comparison with the experimental data. All of the masses are in units of GeV.

	m_0	b_0	b_D	b_F
Fit	0.88(FIX)	−0.6232(1)	0.0570(1)	−0.4022(7)

	m_N	m_Λ	m_Σ	m_Ξ
Fit	0.9392	1.1157	1.1862	1.3272
Exp.	0.938925(645)	1.115683(6)	1.19315(430)	1.31828(343)

addition to m_0 appear in the baryon masses. Although the physical baryon masses can be accurately reproduced, the study in Ref. [47] showed that it is not possible to provide a satisfactory description of the LQCD baryon masses up to this order. In addition, the constraints from baryon masses to meson-baryon scattering will be very weak because there are 24 combinations of LECs in the meson-baryon scattering up to $\mathcal{O}(p^3)$.

Taking all these into account, we calculate the baryon masses up to $\mathcal{O}(p^3)$ in the present work. Using the chiral limit baryon mass determined in Ref. [47], $m_0 = 0.880$ GeV, we determine b_0, b_D, b_F by fitting to the experimental octet baryon masses, with the pseudoscalar decay constants fixed as explained above. The resulting LECs and the fitted octet baryon masses are given in Table VII.

Compared to the fit up to $\mathcal{O}(p^3)$ to the scattering phase shifts, a combined fit of the baryon masses and scattering amplitudes yields a slightly worse description of the scattering phase shifts to some extent (see Tables VIII–X). Particularly, the fitting results are worse in the KN channel where the χ^2/d.o.f. increases by a factor of about 4 with larger error bands. This is understandable as the number of free LECs decreases. Despite this, as one can see from Figs. 7 and 8, the negative effects do not spoil the description. For the p wave, the descriptions of the phase shifts are of very similar quality, whether one fixes b_0, b_D, b_F and treats them as free LECs. For the s wave, the differences are rather moderate, particularly in the low energy region. This study indicates that the EOMS BChPT is able to describe the baryon masses and meson-baryon scattering simultaneously, as it should be. Nevertheless, as mentioned at the beginning of this section, to draw a firm conclusion, more systematic studies are needed.

As for the sigma terms, we find that meson-baryon scattering up to $\mathcal{O}(p^3)$ is not very useful at this moment because the tree level contributions at $\mathcal{O}(p^3)$ in the KN channels are neglected, leading to unusually large b_D, b_F compared to an independent study of the baryon masses in, e.g., Ref. [47]. Thus, we will refrain from performing such a study here.

TABLE IX. LECs in the $I = 0$ KN channel with $\beta_4 = b_0 - b_F$ fixed by fitting to the baryon masses.

	β_1 [GeV^{-1}]	β_2 [GeV^{-2}]	β_3 [GeV^{-1}]	β_4 [GeV^{-1}]	χ^2/d.o.f.
$\mathcal{O}(p^2)$	−0.284(1)	0.144(0)	0.443(3)	−0.221	4.66
$\mathcal{O}(p^3)^*$	−0.582(11)	0.153(3)	0.601(5)	−0.221	3.93

TABLE X. LECs in the $I = 1$ KN channel with $\gamma_4 = b_0 + b_D$ fixed by fitting to the baryon masses.

	γ_1 [GeV^{-1}]	γ_2 [GeV^{-2}]	γ_3 [GeV^{-1}]	γ_4 [GeV^{-1}]	χ^2/d.o.f.
$\mathcal{O}(p^2)$	−0.236(11)	−0.033(3)	0.246(5)	−0.566	1.45
$\mathcal{O}(p^3)^*$	−0.604(15)	0.364(4)	0.588(6)	−0.566	2.24

C. Scattering lengths

Scattering lengths, also known as s-wave threshold parameters, can be predicted with the LECs determined above. The general form of the effective range expansion reads

$$|\mathbf{p}|^{2l+1}\cot\delta^I_{l\pm} = \frac{1}{a^I_{l\pm}} + \frac{1}{2}r^I_{l\pm}|\mathbf{p}|^2 + \sum_{n=2}^{\infty} v^I_{n,l\pm}|\mathbf{p}|^{2n}, \tag{25}$$

where $|\mathbf{p}|$ refers to the three-momentum of the baryon in the c.m. frame, ℓ is the angular momentum, a is the threshold parameter, r is the effective range, and v_n are the shape parameters. We can easily obtain the expression of threshold parameters from Eq. (25) by taking the limit of $|\mathbf{p}| \to 0$ as

$$a^I_{l\pm} = \lim_{|\mathbf{p}|\to 0}\frac{\tan\delta^I_{l\pm}}{|\mathbf{p}|^{2l+1}} = \lim_{|\mathbf{p}|\to 0}\frac{\mathrm{Re}f^I_{l\pm}}{|\mathbf{p}|^{2l}}. \tag{26}$$

With the scattering amplitudes obtained in ChPT, one can easily compute the $\ell = 0$ scattering lengths. The corresponding results for the πN and $\bar{K}N$ channels are collected in Table XI.

It is clear that our results based on the EOMS scheme are in very good agreement with the experimental data and the HB results, while the IR results [14] seem to be compatible with data only in the KN channels. We note that for the two πN channels, the LO scattering lengths, to which no

TABLE VIII. LECs in the πN channel with $\alpha_4 = b_0 + \frac{b_D}{2} + \frac{b_F}{2}$ fixed by fitting to the baryon masses.

α_1 [GeV^{-1}]	α_2 [GeV^{-2}]	α_3 [GeV^{-1}]	α_4 [GeV^{-1}]	α_5 [GeV^{-4}]	α_6 [GeV^{-2}]	α_7 [GeV^{-3}]	α_8 [GeV^{-2}]	χ^2/d.o.f.
−7.41(7)	1.56(2)	1.33(1)	−0.80	0.63(2)	3.18(6)	1.45(3)	−0.096(122)	1.26

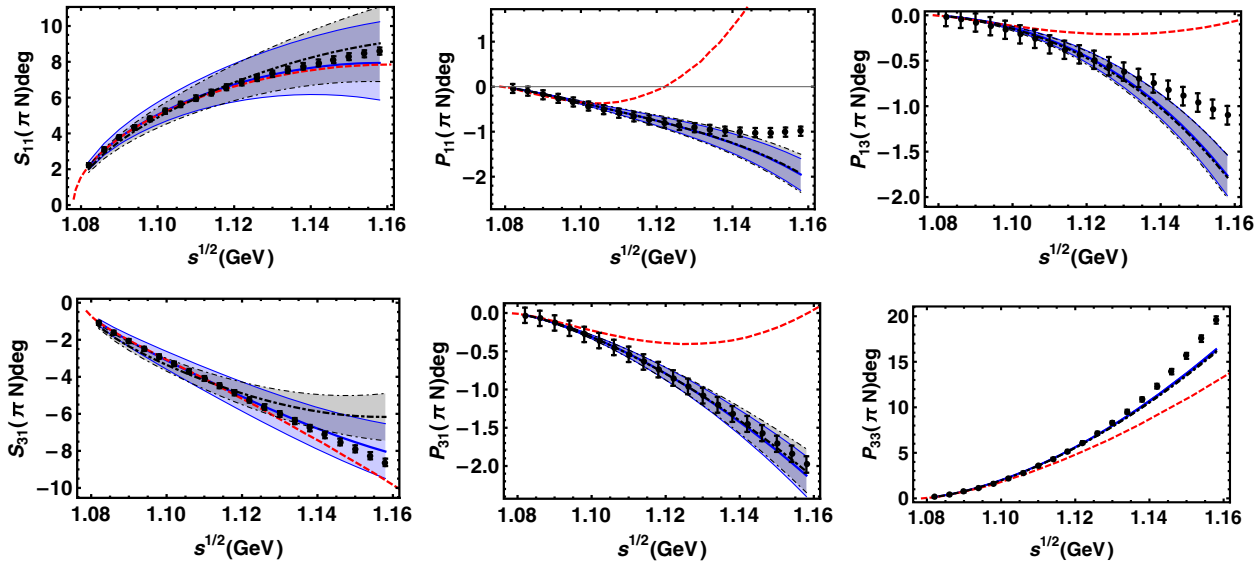

FIG. 7. Same as Fig. 5, but the black dot-dashed lines associated with the grey bands denote the EOMS results and their errors with b_0, b_D, and b_F fixed by fitting to the physical (isospin averaged) octet baryon masses at NNLO. In some partial waves, the error bands are of the size of the thickness of the lines.

unknown LECs contribute, are already compatible with the experimental data. Meanwhile the contributions of the two consecutive orders decrease order by order. Compared to the HB case [16]: $a_{\pi N}^{3/2}(\mathcal{O}(p^2)) = 0.05$ fm, $a_{\pi N}^{3/2}(\mathcal{O}(p^3)) = -0.05$ fm and $a_{\pi N}^{1/2}(\mathcal{O}(p^2)) = 0.05$ fm, $a_{\pi N}^{1/2}(\mathcal{O}(p^3)) = -0.03$ fm, the EOMS results decrease much faster, indicating that the scattering amplitudes in this covariant framework converge faster than in the nonrelativistic calculation close to threshold, and the improvement is significant. In the KN channels, one can see that the NLO results can already describe the experimental data. The improvements from $\mathcal{O}(p^3)$ are so tiny that they can be neglected. However, different from the πN channels, the LO scattering lengths in the KN channels are far from the corresponding experimental data. As a consequence, relatively large contributions from NLO and NNLO are naturally expected. Indeed our calculations yield extremely large values at $\mathcal{O}(p^2)$ and $\mathcal{O}(p^3)^*$ with significant cancellations. All of these point to an unsatisfying convergence even very close to threshold in the KN channels.

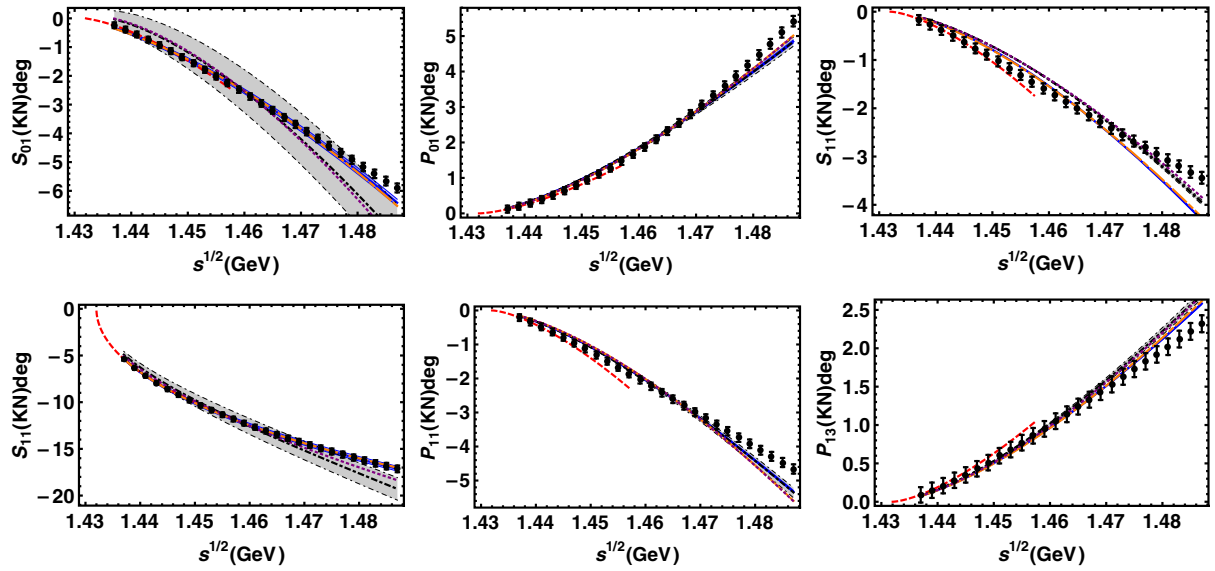

FIG. 8. Same as Fig. 6, but the purple dotted lines and black dot-dashed lines denote the $\mathcal{O}(p^2)$ and $\mathcal{O}(p^3)^*$ results in the EOMS scheme with b_0, b_D, and b_F fixed by fitting to the physical (isospin averaged) octet baryon masses at NNLO. The grey bands correspond to the uncertainties of the $\mathcal{O}(p^3)^*$ results propagated from the uncertainties of the LECs. The error bands of $\mathcal{O}(p^2)$ results are not shown here to make the figures easier to read. In some partial waves, the error bands are of the size of the thickness of the lines.

TABLE XI. πN and KN scattering lengths in units of fm. Note that we did not associate any uncertainties to the $\mathcal{O}(p^3)^*$ contributions of the KN channel because we have not included the tree level contributions at this order for the KN channels.

Channel	$\mathcal{O}(p^1)$	$\mathcal{O}(p^2)$	$\mathcal{O}(p^3)$	Total	Huang (HB) [16]	Mai (IR) [14]	Expt.
$a_{\pi N}^{3/2}$	−0.126	0.026(11)	−0.011(8)	−0.111(16)	−0.110(2)	−0.04(7)	−0.125(3) [72]
$a_{\pi N}^{1/2}$	0.212	0.025(10)	0.003(16)	0.240(22)	0.240(2)	0.07(7)	$0.250^{+0.006}_{-0.004}$ [72]
$a_{KN}^{1}(\mathcal{O}(p^2))$	−0.476	0.149(1)	⋯/⋯	−0.327(1)	−0.330(5)	−0.33(32)	−0.33 [59]
$a_{KN}^{0}(\mathcal{O}(p^2))$	0.043	−0.057(2)	⋯/⋯	−0.014(2)	0.000(4)	0.02(64)	0.02 [59]
$a_{KN}^{1}(\mathcal{O}(p^3)^*)$	−0.476	1.067(5)	−0.919	−0.328(5)	⋯/⋯	⋯/⋯	⋯/⋯
$a_{KN}^{0}(\mathcal{O}(p^3)^*)$	0.043	0.164(2)	−0.219	−0.012(2)	⋯/⋯	⋯/⋯	⋯/⋯

Nonetheless, one should keep in mind that we have neglected the $\mathcal{O}(p^3)$ tree level contribution. To draw a firm conclusion, more experimental data or lattice simulations are strongly needed. More discussions can be found in the following subsection.

D. Convergence of BChPT

The convergence of SU(3) BChPT has remained an issue of heated debate for many years. See, e.g., Ref. [73] for early discussions, and Refs. [48,74] for more recent studies of baryon magnetic moments and masses. From the latter studies, it seems that the EOMS scheme can speed up the convergence of BChPT, particularly, in the SU(3) sector. Nonetheless, even in the EOMS scheme, the convergence turns out to be relatively slow. The origin of this slow convergence in the SU(3) sector is the large expansion parameter $\frac{M_K}{\Lambda_{\chi PT}}$, which is approximately $1/2$ in the physical world. For a LQCD simulation, the situation can become even worse.

The discussion on the convergence of BChPT for meson-baryon scattering can be dated back to the first attempt in the HB scheme by M. Mojžiš [75] where the convergence of threshold parameters was studied. Afterwards N. Fettes *et al.* [58] worked out the pion-nucleon scattering amplitudes up to $\mathcal{O}(p^3)$. Their calculation implies that the third-order contributions are in general small in the lower energy region, while there exist large cancellations for higher energies. However, the discussion of convergence is rather limited, and no firm conclusion could be drawn there. The situation was significantly improved once the full one-loop results became available [76]. They concluded that the contributions from the fourth order are, in most partial waves, indeed not large, indicating the convergence of BChPT. Recently, the discussion on this issue based on SU(3) HBChPT was performed in Refs. [15,16] up to $\mathcal{O}(p^3)$, where a conclusion very similar to those in SU(2) was drawn.

As is well known, the HB ChPT recovers a neat power counting rule at a cost of manifestly Lorentz covariance. It suffers from the deficiency that the corresponding perturbation series fail to converge in parts of the low-energy region [36]. Thus, an analysis based on covariant BChPT was strongly needed. In Ref. [41], the πN scattering amplitudes were calculated up to $\mathcal{O}(p^3)$ in SU(2) with the EOMS scheme. The authors pointed out that the convergence of the Δ-less amplitudes is questionable because there exists a large cancellation between $\mathcal{O}(p^2)$ and $\mathcal{O}(p^3)$ in almost all partial waves. However, including Δ as an explicit degree of freedom, the amplitudes turn out to present a natural convergence from subthreshold up to energies well above threshold. Very soon after this work, Chen *et al.* showed [42] that after promoting the calculation to $\mathcal{O}(p^4)$, the convergence pattern is reasonable even without Δ. Later in Ref. [43], a full third order calculation with an explicit Δ is performed. More recent studies, such as those of Refs. [41,44,46], further confirmed that the convergence pattern is visibly improved in a covariant scheme via a detailed study on threshold and subthreshold parameters, associated with the extracted LECs. They also highlighted the improvements by taking the contributions of resonances such as Δ and Roper into consideration.

It is interesting to check the convergence pattern in SU(3) as well. Nevertheless, one has to be cautious about any conclusion drawn from a leading one-loop study such as the present one. We show the phase shifts of each order in Fig. 9 for the πN channels and Fig. 10 for the KN channels. For the two π-N S waves, the LO contribution itself describes the behavior of phase shifts very well in subthreshold regions, while the NLO and NNLO terms only provide visible effect at higher energies. Especially in the S_{11} partial wave, the contributions decrease order by an order well above the threshold, indicating a reasonable convergence. On the other hand, for all the P waves, the contributions from the NNLO terms are smaller than those from the NLO terms. The LO terms are now approximately the same size as NLO or even smaller because the partial wave decomposition filters out the LO contact terms. In particular, the ratio of the NNLO over NLO terms can be lower than $1/2$ for the two $J=\frac{3}{2}$ partial waves in quite a wide region above the threshold. Despite the cancellation of the NLO and NNLO terms in these partial waves, these smaller ratios actually indicate a reasonable convergence. For the rest of the partial waves, we find a ratio of 0.7–0.8 even very close to the threshold, implying a sizable cancellation and, thus, a much slower convergence.

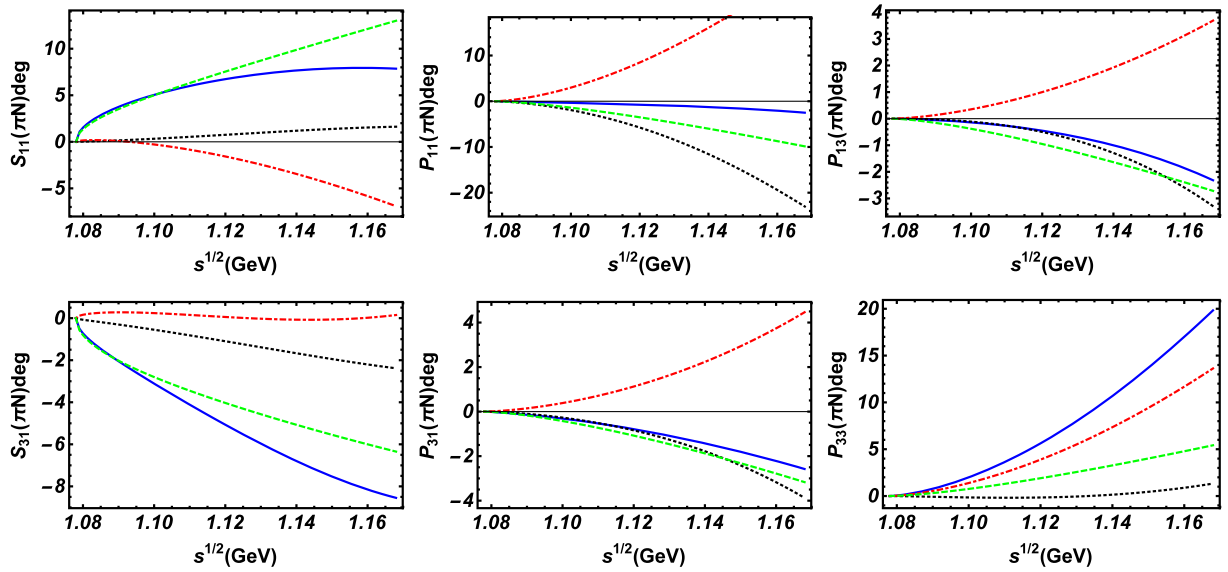

FIG. 9. Order by order decomposition of the πN phase shifts. The blue lines donate the total results, while those of the $\mathcal{O}(p)$, $\mathcal{O}(p^2)$, and $\mathcal{O}(p^3)$ are represented by the green-dashed, red-dot-dashed, and black-dotted lines, respectively.

For the KN channels, the LO results are in general quite small. This is not only because of the partial wave decomposition, but also because the LO Born term can only contribute via the u channel. In the two S waves, the third order contribution is compatible with the second order and the large cancellation points to a questionable convergence. However, for most P waves except P_{13}, the second order contribution dominates the behavior and the third order contribution is significantly smaller than the second order, implying a reasonable convergence, if we ignore the small LO contributions.

In general, we do not find a fast decrease of higher order contributions and the conclusion on the convergence to be drawn here is quite similar to that in SU(2). However, we would like to point out that in some P waves for both the πN and KN channels, the chiral expansions seem to convergence at least near the threshold if we only focus on the NLO and NNLO contributions. We ascribe the slower convergence of the two S waves in the KN channels partially to the fact that we have not taken into account the $\mathcal{O}(p^3)$ tree level contributions. Inspired by the SU(2) studies, we expect that the contributions of the decuplet

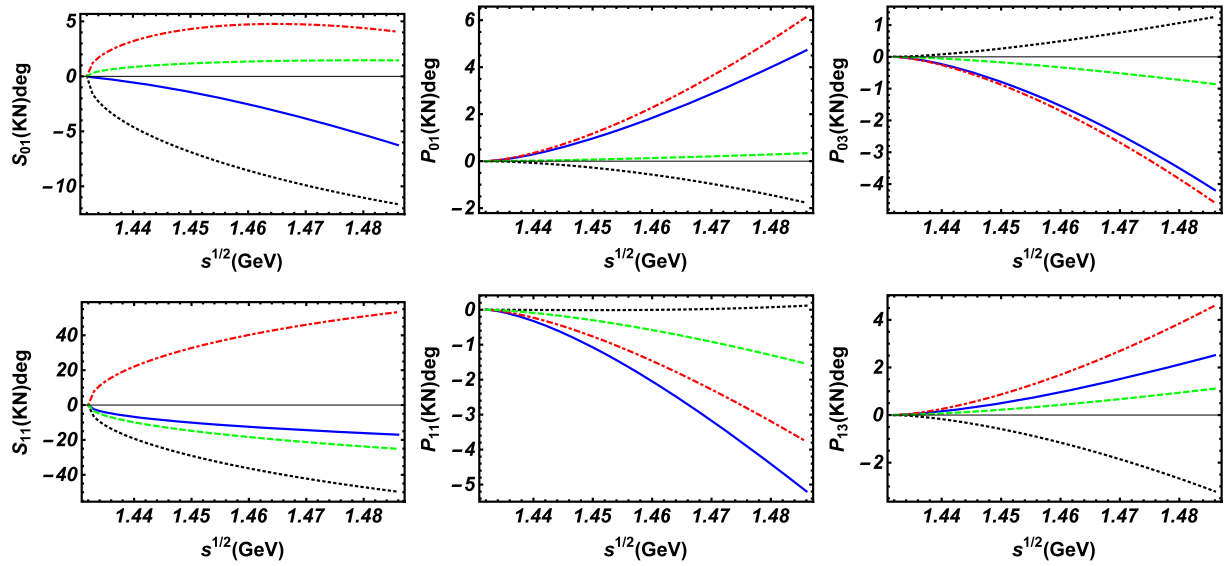

FIG. 10. Order by order decomposition of the KN phase shifts. The blue lines donate the total results, while those of the $\mathcal{O}(p)$, $\mathcal{O}(p^2)$, and $\mathcal{O}(p^3)^*$ are represented by the green-dashed, red-dot-dashed, and black-dotted lines, respectively.

could significantly improve the convergence pattern at least at $\mathcal{O}(p^3)$. Meanwhile, a calculation up to the full one loop order is needed to test the convergence of SU(3) BChPT.

IV. SUMMARY AND OUTLOOK

In this work, we performed a SU(3) study of the meson-baryon elastic scattering up to $\mathcal{O}(p^3)$ in covariant baryon chiral perturbation theory. Due to lack of experimental data, we focus only on the $\pi N^{I=3/2,1/2}$ and $KN^{I=0,1}$ channels. We applied the extended-on-mass-shell (EOMS) scheme to restore the power counting and determined the corresponding low energy constants by fitting to the experimental phase shifts. We achieved a pretty good description in these channels simultaneously up to 1.16 GeV for πN and 1.49 GeV for KN. For the πN channels, our study in SU(3) shows a compatible description as that in SU(2) and much better compared to the HB SU(3) results. Our results showed that different from the HB case, the inclusion of the strangeness in the covariant framework does not affect much the description of the pion-nucleon scattering. For the KN channels, we found that with only phase shifts one can not uniquely determine all the LECs. Nevertheless, neglecting the $\mathcal{O}(p^3)$ tree level contributions, we obtained a description in good agreement with the experimental data.

We attempted a combined study of the baryon masses and meson-baryon scattering up to $\mathcal{O}(p^3)$. We first determined b_0, b_F, b_D using the baryon masses and then kept them fixed in the fitting of the partial wave phase shifts. Our study showed indeed that the EOMS BChPT can describe simultaneously the baryon masses and meson-baryon scattering, but a firm conclusion needs more systematic studies up to higher orders.

The predicted scattering lengths for the πN and KN channels are in good agreement with the HB results and the experimental data. In addition, we explored the convergence of BChPT in meson-baryon scattering. The large cancellation between the NLO and NNLO contributions implies an unsatisfying convergence rate, similar to that of the SU(2) sector up to $\mathcal{O}(p^3)$ without the $\Delta(1232)$ being taken into account. On the other hand, since in the one baryon sector, chiral orders increase by a unit of 1, it might well be the case that one will see cancellations among the contributions of even and odd adjacent orders, as one already noted in the study of decuplet masses.

The predicted phase shifts and scattering lengths for other channels listed in Table II for the case of $\mathcal{O}(p^3)^*$ should be taken with caution since the $\mathcal{O}(p^3)$ LECs are not fully determined. Thus additional data, such as the cross sections in the $\bar{K}N$ channel, ought to be taken into account. As the interaction in this channel is by nature nonperturbative, tiled to the existence of a shallow bound state of $\bar{K}N$, the $\Lambda(1405)$, we leave such a study to a future work.

ACKNOWLEDGMENTS

We thank Ulf-G. Meißner for a careful reading of the manuscript and for many useful comments. This work is partly supported by the National Natural Science Foundation of China under Grants No. 11522539, No. 11735003, and No. 11775099, and the Fundamental Research Funds for the Central Universities. X. L. R. and M. L. D. acknowledge supports form DFG and NSFC through funds provided to the Sino-German CRC 110 "Symmetries and the Emergence of Structure in QCD" (Grant No. TRR110).

APPENDIX A: TREE LEVEL CONTACT TERMS

In this subsection, we list the contributions of the tree-level contact terms. To simplify the expressions, we first define

$$\nu_\pi = (-s + {m_N}^2 + {m_\pi}^2)^2 + (m_N{}^2 + m_\pi{}^2 - u)^2,$$
$$\nu_K = (-s + {m_N}^2 + {m_K}^2)^2 + (m_N{}^2 + m_K{}^2 - u)^2. \quad \text{(A1)}$$

The contributions in the respective channels are

(i) $\pi N^{I=3/2}$

$$B_{\pi N}^{I=3/2} = -\frac{1}{2f^2} + \frac{2(s-u)(b_5+b_6+b_7+b_8)}{f^2} - \frac{8m_N(c_1+c_2)}{f^2} + \frac{4(d_2\nu_\pi + d_4(t-2{m_\pi}^2) - 2d_{49}{m_\pi}^2)}{f^2} - \frac{8m_N(s-u)(d_{10}+d_8)}{f^2}, \quad \text{(A2)}$$

$$A_{\pi N}^{I=3/2} = \frac{2{m_\pi}^2(-2b_0+b_1+b_2+b_3+2b_4-b_D-b_F) - t(b_1+b_2+b_3+2b_4)}{f^2} + \frac{2(s-u)(c_1+c_2)}{f^2} + \frac{2(s-u)^2(d_{10}+d_8)}{f^2}. \quad \text{(A3)}$$

(ii) $\pi N^{I=1/2}$

$$B_{\pi N}^{I=1/2} = \frac{1}{f^2} + \frac{2(s-u)(b_5+b_6+b_7+b_8)}{f^2} + \frac{16m_N(c_1+c_2)}{f^2} + \frac{8(-d_2\nu_\pi + d_4(2{m_\pi}^2 - t) + 2d_{49}{m_\pi}^2)}{f^2} - \frac{8m_N(s-u)(d_{10}+d_8)}{f^2}, \tag{A4}$$

$$A_{\pi N}^{I=1/2} = \frac{2{m_\pi}^2(-2b_0+b_1+b_2+b_3+2b_4-b_D-b_F) - t(b_1+b_2+b_3+2b_4)}{f^2} - \frac{4(s-u)(c_1+c_2)}{f^2} + \frac{2(s-u)^2(d_{10}+d_8)}{f^2}. \tag{A5}$$

(iii) $KN^{I=1}$

$$B_{KN}^{I=1} = -\frac{1}{f^2} + \frac{2(2b_5+2b_7+b_8)(s-u)}{f^2} - \frac{4m_N(4c_2+c_3)}{f^2} - \frac{8m_N(s-u)(d_{10}+d_7+d_8)}{f^2} + \frac{4(\nu_K(-d_1+d_2+d_3) + 2{m_K}^2(-d_4+d_{48}-d_{49}+d_5+d_{50}-d_6) + t(d_4-d_5+d_6))}{f^2}, \tag{A6}$$

$$A_{KN}^{I=1} = \frac{4{m_K}^2(-b_0+b_1+b_2+b_4-b_D) - 2t(b_1+b_2+b_4)}{f^2} + \frac{(s-u)(4c_2+c_3)}{f^2} + \frac{2(s-u)^2(d_{10}+d_7+d_8)}{f^2}. \tag{A7}$$

(iv) $KN^{I=0}$

$$B_{KN}^{I=0} = \frac{2(b_8-2b_6)(s-u)}{f^2} + \frac{4m_N(4c_1+c_3)}{f^2} - \frac{8m_N(s-u)(d_{10}+d_7-d_8)}{f^2} + \frac{4(-\nu_K(d_1+d_2+d_3) + 2{m_K}^2(d_4+d_{48}+d_{49}+d_5-d_{50}+d_6) - t(d_4+d_5+d_6))}{f^2}, \tag{A8}$$

$$A_{KN}^{I=0} = \frac{4{m_K}^2(-b_0-b_3+b_4+b_F) + 2t(b_3-b_4)}{f^2} - \frac{(s-u)(4c_1+c_3)}{f^2} + \frac{2(s-u)^2(d_{10}+d_7-d_8)}{f^2}. \tag{A9}$$

APPENDIX B: TREE LEVEL BORN DIAGRAMS

Once simplified with the on-shell condition, the amplitude for the Born diagrams could be rewritten as

$$B_{\mathrm{Born}}(s, B_i, B_f, P) = -\frac{s + m_P(m_f+m_i) + m_f m_i}{s - {m_P}^2},$$
$$A_{\mathrm{Born}}(s, B_i, B_f, P) = -\frac{m_P(-2s + {m_f}^2 + {m_i}^2) + (m_f+m_i)(m_f m_i - s)}{2(s-{m_P}^2)}, \tag{B1}$$

where s is the invariant mass squared, m_i and m_f are the masses of the initial and final baryons, B_i, B_f, P are the incoming, outgoing, propagating baryons respectively. For a crossed Born diagram, one can obtain the amplitude from the corresponding direct one with the following replacement $s \to u$.

For the d_{45}, d_{46}, d_{47} terms, the expressions are slightly different

$$B^2_{\rm Born}(s,B_i,B_f,P)=\frac{m_i+m_P}{s-{m_P}^2},\qquad A^2_{\rm Born}(s,B_i,B_f,P)=\frac{-2s+m_P(m_f-m_i)+m_f m_i+{m_i}^2}{2(s-{m_P}^2)}. \tag{B2}$$

For the A parts of the Born terms, one would need to perform two replacements

$$B(s)\leftrightarrow A(s),\qquad B(u)\leftrightarrow -A(u). \tag{B3}$$

The contributions of the Born diagrams are

(i) $\pi N^{I=3/2}_{\rm Born}$

$$B^{I=3/2}_{\pi N}=-\frac{B(u,N,N,N)(D+F)^2}{2f^2}+\frac{4B(u,N,N,N)(D+F)(2d_{38}{m_K}^2-d_{38}{m_\pi}^2+2d_{40}{m_K}^2+d_{40}{m_\pi}^2+2d_{44}{m_\pi}^2)}{f^2}$$
$$-\frac{4{m_\pi}^2B^2(u,N,N,N)(D+F)(d_{45}+d_{46})}{f^2}. \tag{B4}$$

(ii) $\pi N^{I=1/2}_{\rm Born}$

$$B^{I=1/2}_{\pi N}=\frac{(D+F)^2(3B(s,N,N,N)+B(u,N,N,N))}{4f^2}-\frac{2(D+F)(3B(s,N,N,N)+B(u,N,N,N))}{f^2}(2d_{38}{m_K}^2-d_{38}{m_\pi}^2$$
$$+2d_{40}{m_K}^2+d_{40}{m_\pi}^2+2d_{44}{m_\pi}^2)+\frac{2{m_\pi}^2(D+F)(d_{45}+d_{46})(3B^2(s,N,N,N)+B^2(u,N,N,N))}{f^2}. \tag{B5}$$

(iii) $KN^{I=1}_{\rm Born}$

$$B^{I=1}_{KN}=-\frac{B(u,N,N,\Lambda)(D+3F)^2+3B(u,N,N,\Sigma)(D-F)^2}{12f^2}$$
$$-\frac{2}{3f^2}({m_\pi}^2(B(u,N,N,\Lambda)(D+3F)(2d_{38}+d_{39}-2d_{40}+d_{41})+3B(u,N,N,\Sigma)(F-D)(d_{39}+d_{41}))$$
$$-2{m_K}^2(B(u,N,N,\Lambda)(D+3F)(2d_{38}+2d_{40}-d_{41}-d_{43}+2d_{44})-3B(u,N,N,\Sigma)(F-D)(d_{41}+d_{43})))$$
$$-\frac{2{m_K}^2(B^2(u,N,N,\Lambda)(D+3F)(d_{45}+3d_{46})-3B^2(u,N,N,\Sigma)(F-D)(d_{45}-d_{46}))}{3f^2}. \tag{B6}$$

(iv) $KN^{I=0}_{\rm Born}$

$$B^{I=0}_{KN}=\frac{B(u,N,N,\Lambda)(D+3F)^2-9B(u,N,N,\Sigma)(D-F)^2}{12f^2}$$
$$-\frac{2}{3f^2}(2{m_K}^2(B(u,N,N,\Lambda)(D+3F)(2d_{38}+2d_{40}-d_{41}-d_{43}+2d_{44})$$
$$+9B(u,N,N,\Sigma)(F-D)(d_{41}+d_{43}))$$
$$-{m_\pi}^2(B(u,N,N,\Lambda)(D+3F)(2d_{38}+d_{39}-2d_{40}+d_{41})-9B(u,N,N,\Sigma)(F-D)(d_{39}+d_{41})))$$
$$+\frac{2{m_K}^2(B^2(u,N,N,\Lambda)(D+3F)(d_{45}+3d_{46})+9B^2(u,N,N,\Sigma)(F-D)(d_{45}-d_{46}))}{3f^2}. \tag{B7}$$

[1] G. Hohler, in *Landolt-Börnstein*, edited by H. Schopper (Springer, Berlin, 1983), Vol. 9b2.
[2] A. Bottino, F. Donato, N. Fornengo, and S. Scopel, Astropart. Phys. **13**, 215 (2000).
[3] J. R. Ellis, K. A. Olive, Y. Santoso, and V. C. Spanos, Phys. Rev. D **71**, 095007 (2005).
[4] J. R. Ellis, K. A. Olive, and C. Savage, Phys. Rev. D **77**, 065026 (2008).
[5] E. Massot, J. Margueron, and G. Chanfray, Europhys. Lett. **97**, 39002 (2012).
[6] H.-J. Schulze and T. Rijken, Phys. Rev. C **84**, 035801 (2011).
[7] J. N. Hu, A. Li, H. Toki, and W. Zuo, Phys. Rev. C **89**, 025802 (2014).
[8] T. Miyatsu, S. Yamamuro, and K. Nakazato, Astrophys. J. **777**, 4 (2013).
[9] P. Demorest, T. Pennucci, S. Ransom, M. Roberts, and J. Hessels, Nature (London) **467**, 1081 (2010).
[10] J. Antoniadis *et al.*, Science **340**, 1233232 (2013).
[11] N. Kaiser, Phys. Rev. C **64**, 045204 (2001); **73**, 069902(E) (2006).
[12] Y. R. Liu and S. L. Zhu, Phys. Rev. D **75**, 034003 (2007).
[13] Y. R. Liu and S. L. Zhu, Eur. Phys. J. C **52**, 177 (2007).
[14] M. Mai, P. C. Bruns, B. Kubis, and U. G. Meißner, Phys. Rev. D **80**, 094006 (2009).
[15] B. L. Huang and Y. D. Li, Phys. Rev. D **92**, 114033 (2015); **95**, 019903(E) (2017).
[16] B. L. Huang, J. S. Zhang, Y. D. Li, and N. Kaiser, Phys. Rev. D **96**, 016021 (2017).
[17] A. Torok, S. R. Beane, W. Detmold, T. C. Luu, K. Orginos, A. Parreño, M. J. Savage, and A. Walker-Loud, Phys. Rev. D **81**, 074506 (2010).
[18] W. Detmold and A. Nicholson, Phys. Rev. D **93**, 114511 (2016).
[19] M. Niiyama *et al.*, Phys. Rev. C **78**, 035202 (2008).
[20] G. Agakishiev *et al.* (HADES Collaboration), Phys. Rev. C **87**, 025201 (2013).
[21] K. Moriya *et al.* (CLAS Collaboration), Phys. Rev. C **87**, 035206 (2013).
[22] K. Moriya *et al.* (CLAS Collaboration), Phys. Rev. C **88**, 045201 (2013); **88**, 049902 (2013).
[23] K. Moriya *et al.* (CLAS Collaboration), Phys. Rev. Lett. **112**, 082004 (2014).
[24] S. Weinberg, Physica (Amsterdam) **96A**, 327 (1979).
[25] J. Gasser and H. Leutwyler, Ann. Phys. (N.Y.) **158**, 142 (1984).
[26] J. Gasser and H. Leutwyler, Nucl. Phys. **B250**, 465 (1985).
[27] J. Gasser, M. E. Sainio, and A. Švarc, Nucl. Phys. **B307**, 779 (1988).
[28] H. Leutwyler, arXiv:hep-ph/9406283.
[29] V. Bernard, N. Kaiser, and U. G. Meißner, Int. J. Mod. Phys. E **04**, 193 (1995).
[30] A. Pich, Rep. Prog. Phys. **58**, 563 (1995).
[31] G. Ecker, Prog. Part. Nucl. Phys. **35**, 1 (1995).
[32] S. Scherer, Adv. Nucl. Phys. **27**, 277 (2003).
[33] V. Bernard, Prog. Part. Nucl. Phys. **60**, 82 (2008).
[34] V. Lensky and V. Pascalutsa, Eur. Phys. J. C **65**, 195 (2010).
[35] E. E. Jenkins and A. V. Manohar, Phys. Lett. B **255**, 558 (1991).
[36] T. Becher and H. Leutwyler, Eur. Phys. J. C **9**, 643 (1999).
[37] J. Gegelia and G. Japaridze, Phys. Rev. D **60**, 114038 (1999).
[38] T. Fuchs, J. Gegelia, G. Japaridze, and S. Scherer, Phys. Rev. D **68**, 056005 (2003).
[39] L. Geng, Front. Phys. **8**, 328 (2013).
[40] J. M. Alarcón, J. Martin Camalich, and J. A. Oller, Phys. Rev. D **85**, 051503 (2012).
[41] J. M. Alarcón, J. Martin Camalich, and J. A. Oller, Ann. Phys. (Amsterdam) **336**, 413 (2013).
[42] Y. H. Chen, D. L. Yao, and H. Q. Zheng, Phys. Rev. D **87**, 054019 (2013).
[43] D. L. Yao, D. Siemens, V. Bernard, E. Epelbaum, A. M. Gasparyan, J. Gegelia, H. Krebs, and U. G. Meißner, J. High Energy Phys. 05 (2016) 038.
[44] D. Siemens, V. Bernard, E. Epelbaum, A. Gasparyan, H. Krebs, and U. G. Meißner, Phys. Rev. C **94**, 014620 (2016).
[45] D. Siemens, J. Ruiz de Elvira, E. Epelbaum, M. Hoferichter, H. Krebs, B. Kubis, and U.-G. Meißner, Phys. Lett. B **770**, 27 (2017).
[46] D. Siemens, V. Bernard, E. Epelbaum, A. M. Gasparyan, H. Krebs, and U. G. Meißner, Phys. Rev. C **96**, 055205 (2017).
[47] X.-L. Ren, L. S. Geng, J. Martin Camalich, J. Meng, and H. Toki, J. High Energy Phys. 12 (2012) 073.
[48] X. L. Ren, L. Geng, J. Meng, and H. Toki, Phys. Rev. D **87**, 074001 (2013).
[49] X. L. Ren, L. S. Geng, and J. Meng, Eur. Phys. J. C **74**, 2754 (2014).
[50] X. L. Ren, L. S. Geng, and J. Meng, Phys. Rev. D **89**, 054034 (2014).
[51] X. L. Ren, L. S. Geng, and J. Meng, Phys. Rev. D **91**, 051502 (2015).
[52] X. L. Ren, K. W. Li, L. S. Geng, B. W. Long, P. Ring, and J. Meng, Chin. Phys. C **42**, 014103 (2018).
[53] K. W. Li, X. L. Ren, L. S. Geng, and B. W. Long, Chin. Phys. C **42**, 014105 (2018).
[54] J. Song, K. W. Li, and L. S. Geng, Phys. Rev. C **97**, 065201 (2018).
[55] K. W. Li, T. Hyodo, and L. S. Geng, Phys. Rev. C **98**, 065203 (2018).
[56] Y. Xiao, L. S. Geng, and X. L. Ren, Phys. Rev. C **99**, 024004 (2019).
[57] T. Becher and H. Leutwyler, J. High Energy Phys. 06 (2001) 017.
[58] N. Fettes, U. G. Meißner, and S. Steininger, Nucl. Phys. **A640**, 199 (1998).
[59] R. A. Arndt, W. J. Briscoe, I. I. Strakovsky, and R. L. Workman, Phys. Rev. C **74**, 045205 (2006).
[60] J. S. Hyslop, R. A. Arndt, L. D. Roper, and R. L. Workman, Phys. Rev. D **46**, 961 (1992).
[61] M. Hoferichter, J. Ruiz de Elvira, B. Kubis, and U. G. Meißner, Phys. Rep. **625**, 1 (2016).
[62] J. A. Oller, M. Verbeni, and J. Prades, arXiv:hep-ph/0701096.
[63] J. A. Oller, M. Verbeni, and J. Prades, J. High Energy Phys. 09 (2006) 079.
[64] M. Frink and U. G. Meißner, Eur. Phys. J. A **29**, 255 (2006).

[65] M. Frink and U. G. Meißner, J. High Energy Phys. 07 (2004) 028.
[66] X. L. Ren, L. Alvarez-Ruso, L. S. Geng, T. Ledwig, J. Meng, and M. J. Vicente Vacas, Phys. Lett. B **766**, 325 (2017).
[67] A. van Hameren, C. G. Papadopoulos, and R. Pittau, J. High Energy Phys. 09 (2009) 106.
[68] A. van Hameren, Comput. Phys. Commun. **182**, 2427 (2011).
[69] U. G. Meißner and J. A. Oller, Nucl. Phys. **A673**, 311 (2000).
[70] J. M. Alarcón, J. Martin Camalich, J. A. Oller, and L. Alvarez-Ruso, Phys. Rev. C **83**, 055205 (2011); **87**, 059901(E) (2013).
[71] T. P. Cheng and R. F. Dashen, Phys. Rev. Lett. **26**, 594 (1971).
[72] H. C. Schröder *et al.*, Eur. Phys. J. C **21**, 473 (2001).
[73] V. Bernard, T. R. Hemmert, and U. G. Meißner, Nucl. Phys. **A732**, 149 (2004).
[74] Y. Xiao, X. L. Ren, J. X. Lu, L. S. Geng, and U. G. Meißner, Eur. Phys. J. C **78**, 489 (2018).
[75] M. Mojžiš, Eur. Phys. J. C **2**, 181 (1998).
[76] N. Fettes and U. G. Meißner, Nucl. Phys. **A676**, 311 (2000).